

UN and U₃Si₂ composites densified by spark plasma sintering for accident-tolerant fuels

Bowen Gong^a, Erofili Kardoulaki^b, Kun Yang^a, Andre Broussard^a, Dong Zhao^a, Kathryn Metzger^c, Joshua T. White^b, Michael R. Sivack^c, Kenneth J. McClellan^b, Edward J. Lahoda^c, Jie Lian^{a,d,*}

^a Department of Mechanical, Aerospace and Nuclear Engineering, Rensselaer Polytechnic Institute, USA

^b Los Alamos National Laboratory, USA

^c Westinghouse Electric Company, USA

^d Department of Materials Science & Engineering, Rensselaer Polytechnic Institute, USA

ARTICLE INFO

Keywords:

Composite nuclear fuel
Micro-cracking mitigation
Oxidation resistance
Thermomechanical property

ABSTRACT

Both UN and U₃Si₂ are potential candidates for accident tolerant fuels due to their high fissile element density and exceptional thermal conductivity. However, they display a high susceptibility to oxidation and corrosion in steam environments. UN and U₃Si₂ composites were synthesized by conventional vacuum sintering but suffered significant micro-cracks in the silicide phase due to a mismatch in their thermal expansion. In this work, we report promising results of synthesizing UN-U₃Si₂ composites by spark plasma sintering and the micro-cracks can be significantly mitigated by controlling the cooling. Composite fuel pellets with a density of over 95% theoretical density and a uniform distribution of nitride and silicide phases can be achieved without micro-crack formation. The composite with 50 wt% UN and 50 wt% U₃Si₂ displays simultaneously-enhanced strength and fracture toughness, and possesses excellent thermal conductivity. The onset temperatures of all composites tested through dynamic oxidation testing are close to 540 °C, suggesting significantly improved oxidation resistance than the monolithic UN. These results demonstrate the potential of synergizing UN and U₃Si₂ in composites with enhanced fuel properties.

1. Introduction

After the Fukushima accident, accident tolerant fuels (ATFs) have been actively pursued to enhance fuel performance and improve safety margins of nuclear energy systems [1]. For nuclear fuels, there have been many studies aiming at the design of doped oxide fuels and high fissile density fuels and improvement of their thermomechanical properties [2–6], as well as improving their performance and reliability. Doped UO₂ composite fuels have been developed and tested with diverse microstructures [7,8] and stoichiometries [9,10]. The doping effect in UO₂ has also been of a great interest since a small amount of dopant can generally lead to a significant improvement in the thermomechanical properties of nuclear fuels. Chromia doped UO₂ is a leading concept of the ATF [11,12], and the large-grain size of the doped fuels is expected to improve fission gas retention and plastic deformation behavior. Titania was found to effectively increase the grain size of the sintered

UO₂ samples [13], and BeO doped UO₂ was found to have a higher thermal conductivity [14].

In addition to doped oxide fuels, both silicides and nitrides have been considered as primary fuel forms for ATF applications. U₃Si₂ has a 17% higher uranium density [15] and a much improved thermal conductivity than UO₂ [16–18], making it possible to efficiently release heat from the core to the coolant during normal operation. The thermal conductivity of U₃Si₂ increases with temperature, beneficial to heat transfer at elevated temperature and reducing temperature gradient across fuel matrix and center-line temperature. U₃Si₂ also displays good oxidation resistance in air but has a poor performance in steam [19,20]. Gong et al. [21] reported that the microcrystalline and nanocrystalline U₃Si₂ pellets synthesized by spark plasma sintering (SPS) have an onset temperature of 520 °C and 510 °C respectively, significantly higher than that of UO₂ (~400 °C [22]). Nanocrystalline U₃Si₂ has a much lower oxidation rate than UO₂ [22], possibly due to the strain effect introduced during the

* Corresponding author. Department of Mechanical, Aerospace and Nuclear Engineering, Rensselaer Polytechnic Institute, USA.
E-mail address: lianj@rpi.edu (J. Lian).

sintering process. The slower oxidation rate implies that the fuel can have a higher chance to survive from degradation, maintain its integrity, and at the same time avoid rapid pulverization and washout to the primary loop [23]. Significant progress has been achieved in using metallic additives to improve the oxidation and corrosion resistance of U_3Si_2 fuels. Particularly, Cr doped silicide fuels exhibit excellent oxidation resistance in air with the onset temperature above 600 °C and also show excellent steam oxidation resistance without degradations for 24 h at 360 °C [24], and the fuel shows well-maintained pellet integrity and no pulverization was observed. This is the first promising result for U_3Si_2 -based fuel, showing greatly improved oxidation and corrosion resistance in the steam environment under relevant reactor operating conditions.

Similar to U_3Si_2 , uranium mononitride (UN) is also being actively considered as a concept of ATFs, which has an even higher uranium loading than U_3Si_2 . UN [25–27] possesses higher thermal conductivity that increases with temperature. However, SPS-sintered dense UN specimen display inferior performance against dynamic oxidation with an onset temperature of ~400 °C, lower than that of U_3Si_2 . Both U_3Si_2 and UN have their unique advantages over UO_2 ; however, the synthesis of monolithic UN to high density above 95% is challenging due to its high melting point (~2950 K [15]). The sintering of dense monolithic UN in the traditional way requires a sintering temperature of >2000 °C. At high temperatures, UN may be prone to decompose to metallic uranium and release nitrogen and can potentially be oxidized to UO_2 , especially under an environment with a low content of nitrogen [28]. On the other hand, U_2N_3 can also form during the sintering, the content of which can be as high as 34% with very fine starting powder [29]. Using SPS as an advanced fuel manufacturing technology, dense UN pellets can be fabricated at a lower temperature of 1600 °C within a few minutes [30], enabling well-controlled fuel microstructure, phase and stoichiometry.

Extensive efforts are ongoing to design composite fuels targeting the improvement of the fuel properties by synergizing advantages of heterogeneous components together for an advanced fuel form. For example, $\text{U}_3\text{Si}_2\text{-UO}_2$ [16] composites with various compositions and microstructures were fabricated with SPS, and it was found that the composites with 50 wt% UO_2 simultaneously has an excellent oxidation resistance and high fracture toughness. $\text{UO}_2\text{-UN}$ composites were also fabricated [31], and it was found that the incorporation of UO_2 enhanced the oxidation resistance of the UN matrix. These findings suggest that the incorporation of two nuclear fuels can indeed combine the advantages of both phases/compositions to synergistically improve their properties and performance.

The UN- U_3Si_2 composite was also synthesized by conventional sintering, and their microstructure and fuel properties were characterized. In the composite, U_3Si_2 can be utilized as a second phase to assist the sintering, which has several distinct merits. Firstly, it was confirmed [32] that the temperature required for sintering dense UN is greatly reduced, suggesting that the incorporation of U_3Si_2 indeed can improve the sinterability of the composite. Secondly, the U_3Si_2 phase has a higher oxidation resistance, and the incorporation of U_3Si_2 may improve the oxidation resistance of the UN- U_3Si_2 [33]. However, the previously-reported UN- U_3Si_2 composites sintered with liquid phase sintering [33] and SPS [34] both display defects such as micro-cracks and ternary phases, possibly $\text{U}_{20}\text{Si}_{16}\text{N}_3$ or $\text{U}_3\text{Si}_2\text{N}_2$ [35]. Microcracking occurred in the composites, which was induced by the mismatch in the coefficients of thermal expansion between UN (from 7.51 to $10.65 \times 10^{-6} \text{ K}^{-1}$ within the temperature regime of 298–2523 K) and U_3Si_2 ($\sim 16.1 \times 10^{-6} \text{ K}^{-1}$). An inhomogeneous microstructure was observed with large U_3Si_2 inclusions surrounded by small UN particles, leading to the low density of the sintered composites and poor performance.

This work reports the fabrication of dense UN- U_3Si_2 composites with various U_3Si_2 compositions by SPS with a controlling cooling process to mitigate the potential issue of microcracking. All pellets were sintered at 1450 °C for 10 mins with a density of over 95% theoretical density.

Different contents ranging from 25 wt% to 75 wt% of U_3Si_2 were considered in the UN- U_3Si_2 composites. The impact of different amounts of silicide and nitride phases in the composites on fuel properties was also evaluated. The SPS densified UN- U_3Si_2 composites display uniform microstructures without micro-cracks, and dual phases of UN and U_3Si_2 with a uniform distribution are observed along with a possible ternary phase of U-Si-N. The UN- U_3Si_2 composite pellets display improved thermal-mechanical and oxidation properties as compared with monolithic nitrides or silicides. These findings highlight the potential of combining two or more nuclear fuels to form composites with distinct advantages for advanced fuel designs and enhanced fuel properties.

2. Experimental details

2.1. Powder preparation

The original U_3Si_2 powders were manufactured at Idaho National Laboratory (INL) through the approach of arc melting, which involved mixing of uranium and silicon, multi-step arc melting with various currents, and thermal annealing. The detailed preparation process was documented in Harp [36]. The UN powders were prepared at Los Alamos National Laboratory (LANL) via the carbothermic reduction and nitridization approach. The particle sizes of the as-received U_3Si_2 and UN powders were firstly reduced by a high energy ball milling (HEBM) in order to increase their sinterability. The apparatus used in this work is a planetary micro mill (Pulverisette 7, Idar-Oberstein, Germany), with a ball milling jar made of tungsten carbide (WC) and two 8-mm diameter WC balls. The ball milling process consisted of 44 cycles for each type of powders, with 15-min milling time and 10-min idle time in each cycle. The speed was set to 500 rpm. The powders were then mixed with 4-cycle ball milling to allow a uniform mixture. During the powder preparation, all the handling was performed in a glovebox with a controlled environment, and the oxygen level is maintained below 1 ppm.

2.2. Spark plasma sintering

The synthesis of the composite fuels was performed in a SPS apparatus (Thermal tech® SPS 10-3, Santa Rosa, California), and the sintering temperature was controlled via an infrared thermometer. During the sintering, Ar was used as the protecting atmosphere. A piece of graphite foil was firstly rolled and inserted into the graphite die and was then sprayed with boron nitride (BN) to eliminate the contact between the UN/ U_3Si_2 powders and the inner wall of the die to avoid carbon contamination to the sintered pellets. Around 1 g of well-mixed composite powders were subsequently loaded into the die and manually pressed with two graphite punches from both ends of the die. The whole assembly was wrapped with a piece of graphite felt to reduce heat loss during the sintering process. The powders were pre-pressed with a load of 15 MPa prior to the sintering, and the load gradually increased to 50 MPa, which was held until the end of the synthesis. The heating rate was set to 100 °C/min, and the temperature was set to 1450 °C for all composites. During the sintering, the temperature was constantly measured with a pyrometer. When the sintering temperature was reached, the sample was isothermally held for 10 minutes. To mitigate the microcracking induced by the thermal mismatch between UN and U_3Si_2 , a controlled cooling process was adopted. Specifically, all of the samples were cooled down from the sintering temperature (1450 °C) to 1200 °C with a cooling rate of 50 °C/min, followed by a small period of isothermal holding (5 minutes) at 1200 °C and another controlled cooling with a cooling rate of 100 °C/min to 600 °C, and finally the load was released when the sintering program terminated, and the sample was cooled down gradually in the chamber. The samples were then polished using silicon carbide papers with 240, 600, 1200 grits, and the diamond paste with 9, 3, and 1 μm diamond particle sizes. The physical density of each sample was determined with an Archimedes method and

was compared with the theoretical density (TD) calculated based on the compositions of UN and U₃Si₂ in the composites.

2.3. Microstructure characterization of UN and U₃Si₂ composites

A field-emission scanning electron microscopy (SEM) (Carl Zeiss Supra 55, Jena, Germany) was used to characterize the microstructure of the sintered fuel pellets. Energy dispersed spectroscopy (EDS) (Oxford, UK) was used to perform the elemental analysis and confirm the elemental composition of the sintered composites. A PanAlytical X'Pert diffractometer (Westborough, Massachusetts) with Cu K α irradiation and 1.5406 Å wavelength were used to obtain the XRD pattern and to determine the phase of the pellets. The scanning range is 20–80°, and the scanning step was set to be 0.05°, with a scanning rate of 2 sec/step.

2.4. Oxidation resistance of the composite fuel

A thermogravimetric analysis (TGA) apparatus was used to test the oxidation performance of the composite specimens through dynamic oxidation tests. The model of the TGA used is SDT650 (thermal analysis (TA) instrument, Delaware), which is equipped with a simultaneous differential scanning calorimetry (DSC)/TGA system. During testing, mass change and heat flow were simultaneously recorded as the sample was heated to the desired temperature. Prior to the test, the apparatus was calibrated with the melting point of Zinc. For each dynamic oxidation test, a specimen with a weight being around 30 mg was loaded into an alumina crucible and was covered with a lid to avoid split during the test. The temperature was raised from room temperature to 1000 °C with an increment of 10 °C/min. The testing was terminated when the desired temperature was achieved, and the sample was cooled down gradually. The recorded weight change and the heat flow were plotted with respect to temperature, and the onset temperature was determined based on the method described by Wood [37].

2.5. Mechanical properties measurements of composite fuels

The mechanical properties, specifically hardness and fracture toughness, were determined using a micro-hardness tester (Leco M-400). Around 10 indentations were generated for each sample with a load of 1 kgF (~9.8 N), and each indentation lasted for 15 seconds. The Vickers hardness and fracture toughness were determined based on the measurements of the SEM image of each indentation. The hardness was evaluated through equation (1), where H is hardness, P is the load, and a is the average of the diagonal lengths of the indentation. On the other hand, the fracture toughness was assessed with equation (2) [38], where δ is indenter geometry related parameter, E is Young's modulus, H is the hardness, P is the load, and C is the average value of all crack lengths. 163 GPa was used as the Young's modulus of U₃Si₂, which was calculated with density functional theory (DFT) [39]. 210 GPa was used as the Young's modulus of UN [40]. The Young's modulus of the composites was determined based on the linear combination of the weight ratio of each component.

$$H = 1.854 \frac{P}{a^2} \quad (1)$$

$$K_{IC} = \delta \left(\frac{E}{H} \right)^{0.5} \left(\frac{P}{C^{1.5}} \right) \quad (2)$$

2.6. Evaluation of thermal properties of composite fuels

The thermal diffusivity of the UN + U₃Si₂ composites was measured with a laser flash apparatus (LFA, LFA-457, NETZCH, Bavaria, Germany). The samples prepared for thermal diffusivity measurements were around 8 mm in diameter and 2 mm in thickness. Graphite spray was used to uniformly coat both sides of the sample to improve the laser

energy absorption and emissivity. The LFA chamber was evacuated and backfilled with ultra-high purity (UHP) Ar three times before the testing. The temperature range for each test was from room temperature to 927 °C (1200 K), with an increment of 50 °C. At each testing temperature, a total of 10 measurements were performed, and the average was taken as the thermal diffusivity value. The heating rate was kept at 5 °C/min, and the thermal diffusivity was calculated using the Cape-Lehman model with a pulse correction algorithm. The thermal conductivity was calculated according to equation (3), where α is thermal diffusivity, ρ is the density of the sample, and c_p is the specific heat capacity. The temperature-dependent density was calculated with equation (4) [41], where ρ_0 is the density at T_0 , the reference temperature, and α_p is the thermal expansion coefficient. The temperature-dependent specific heat capacity c_p for UN was found from the literature [25], and for U₃Si₂, c_p was calculated based on equation (5) [42,43]. The specific heat capacity of the composites was determined based on the linear combination and the weight ratio of the two components.

$$\kappa = \alpha \rho c_p \quad (3)$$

$$\rho = \frac{\rho_0}{[1 + \alpha_p(T - T_0)]^3} \quad (4)$$

$$c_p = 140.5 + 0.02582 \times T \quad (5)$$

3. Results and discussion

3.1. Composite UN-U₃Si₂ samples sintered with SPS at 1450 °C for 10 minutes

Previous experiments [44] suggest that dense uranium mononitride samples can be sintered at 1650 °C and 45 MPa for 4 min, or at 1450 °C with a higher pressure and longer holding time. However, the sintering temperature for UN is too high for U₃Si₂, which has a melting point of 1665 °C. In a prior work related to the sintering of U₃Si₂ with SPS [21], it was found that dense U₃Si₂ samples can be sintered at 1000 °C for 5 min. Thus, a sintering temperature of 1450 °C with sintering pressure being 50 MPa and holding time being 10 min was chosen for the synthesis of the composite fuel UN-U₃Si₂ with various amounts of U₃Si₂. A total of three batches of composite fuels were sintered by SPS, with the amount of UN ranging from 25 wt%, 50 wt%, to 75 wt%. The sintered pellets have a density of 96.1%, 96.5%, and 95.1% theoretical density (TD), respectively, where the TD was determined based on the rule of mixture of each composite. Fig. 1 shows the SEM images of the SPS-sintered composite pellets sintered at 1450 °C for 10 min. These images show that the samples with 25% UN and 50% UN (Fig. 1A and B) are dense and uniform, apart from a few small pores. At least three phases can be identified, which are UN, U₃Si₂, and a Si-rich phase. The UN phase is found to be embossed, while the other two phases are recessed underneath the polishing surface, as observed in Ref. [33]. Besides, both UN and U₃Si₂ phases show similar contrasts, which can be demonstrated by the EDS mapping in Fig. 3. Compared to the Si-rich phase, the phases of U₃Si₂ and UN have similar molar mass, thus showing similar contrasts. The UN phase is found to be surrounded by the U₃Si₂ phase, suggesting that U₃Si₂ may provide protection to the UN phase during oxidation. The Si-rich phase displays a darker contrast compared to the UN and U₃Si₂ phase. For the sample with 75% UN, its density is slightly lower than the previous two samples, which can be judged from slightly larger pores. One possible reason is that this sample has a higher amount of UN, which requires a higher sintering temperature to densify. The grain size in the first two samples is not uniform, which can be judged from the coexistence of small grains with an average grain size of 4.5 μm, as well as large grains with an average grain size of 18.3 μm. This might be due to the low sintering temperature compared to the melting point of UN. White et al. [33] fabricated UN + U₃Si₂ composites using a liquid phase sintering technique and observed similar results. The sintering

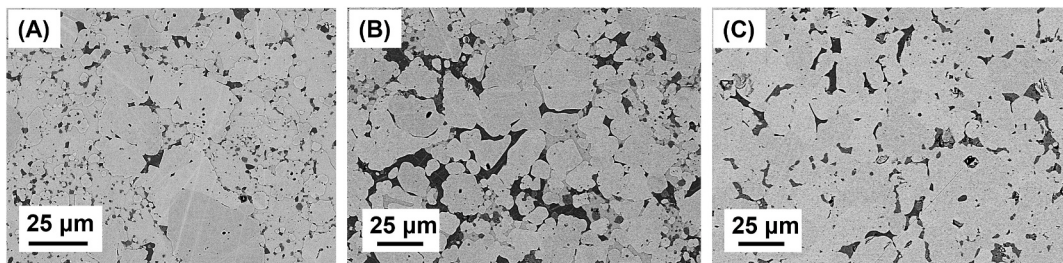


Fig. 1. SEM images showing morphologies of three UN + U₃Si₂ composites densified by SPS: (A) 25 wt% UN + 75 wt% U₃Si₂, (B) 50 wt% UN + 50 wt% U₃Si₂, and (C) 75 wt% UN + 25 wt% U₃Si₂. The UN phase and U₃Si₂ phase are uniformly distributed in the composites. No obvious micro-cracks can be identified for these SPS densified pellets with controlled cooling.

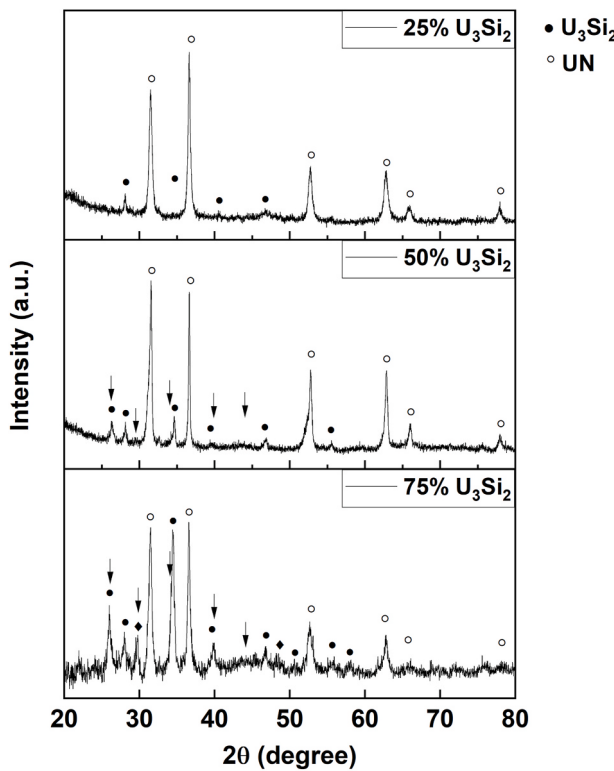


Fig. 2. XRD patterns showing the existence of dual phases U₃Si₂ and UN of the SPS-densified UN + U₃Si₂ composites with different UN contents, with a small amount of ternary phase, possibly U₂₀Si₁₆N₃. The peaks for U₂₀Si₁₆N₃ are marked as arrow.

temperature they used ranged from 1837 K to 2057 K, which is much higher than the sintering temperature required in this work. However, the SEM images revealed that many more pores were observed in their UN + U₃Si₂ composite samples, along with microcracks that can be observed all over the matrix. A Si-rich phase was also observed in their samples, which was possibly U₃Si₅ introduced from the preparation of original powders. It was reported that U₃Si₅ forms even when producing single crystal U₃Si₂ [45]. Johnson et al. [32] fabricated the UN-U₃Si₂ composites using SPS at 1450 °C and 135 MPa and achieved high-density composites with 98% TD. However, the light optical microscopy (LOM) analysis indicates a strong inhomogeneity in the sintered samples with a dendritic structure, featuring of a mixture of regions with various grain sizes and different geometries. The author also observed highly heterogeneous regions that were filled with high-density UN as well as silicide inclusions. Compared to the work from literature, the phases of the composite fuels in this work are quite homogeneous, suggesting a well-controlled microstructure. No obvious micro-cracks can be found in these three batches of composite fuels,

which is distinct from the samples sintered via liquid phase sintering [33]. This seems to suggest that the controlled cooling process applied during the SPS sintering can significantly reduce the microcracking induced from the thermal mismatch, which can also be considered when sintering other composites ceramics using SPS.

Fig. 2 shows the XRD patterns of the composite fuels with 25 wt%, 50 wt%, and 75 wt% U₃Si₂, respectively. In addition to UN and U₃Si₂, peaks of a third phase can be identified, which might correspond to the Si-rich phase, possibly U₂₀Si₁₆N₃ [35], the peaks of which were marked with an arrow in the plot (**Fig. 2**). An unknown phase was also observed by White et al. [33], and it was believed that the peaks belong to a ternary phase of U-Si-N. Different from White and Johnson, no U₃Si₅ was identified from the XRD patterns here. **Fig. 3** shows the EDS mappings of a randomly selected region of each composite sample, from which several observations can be made. Firstly, it can be noticed that the UN and U₃Si₂ phases are uniformly distributed in the matrix, indicating a well-controlled microstructure. Secondly, it can be clearly seen that the UN phase is embossed while the U₃Si₂ phase is recessed under the surface. Thirdly, a Si-rich phase can be observed, which corresponds to the dark-contrast region in the SEM image and the brighter-contrast region in the Si-element EDS result. These regions also display a U-lean characteristic, which can be observed by comparing the U-element and Si-element in EDS result. A fourth phase can be observed from each sample, which is labeled as phase 4 and has a light-gray contrast. This phase corresponds to the oxidized products, the amount of which decreases with the increase of the UN content. To better understand the composition of each phase, a detailed EDS point scan on the sample with 50 wt% U₃Si₂ was conducted, along with the corresponding mapping. The results of the point scan and the elemental mappings are shown in **Fig. 4**, and the point scan results are summarized in **Table 1**. Phases with different contrast can be observed from the SEM image shown in **Fig. 4A**. It is obvious that no micro-cracking can be found, confirming that the micro-cracking can be significantly mitigated with controlled sintering processes. The EDS spectra are shown in **Fig. 4B**, with four elements being indexed, including U, Si, O, and N. There are some extra peaks (not labeled on the plot) that can be indexed to C. Spot 1 and spot 2 are found to be consisted of all four elements U, Si, O, and N, with spot 1 showing a higher ratio of Si and a lower ratio of N. This is probably due to the partial melting of U₃Si₂ during the sintering process. The various contents of Si in different regions can also be observed from the EDS mapping in **Fig. 4D**, where the brighter region corresponds to the Si-rich phase and the darker region to the Si-deficient phase. Spot 3 is located inside an oxidized zone, which can be identified as the bright region in **Fig. 4E**. Point scan results suggest that this is surface oxidation of UN. The matrix can be identified as UN phase, with minimum oxidation. The detailed phase composition of the oxidized product is not currently available, which needs to be further analyzed with EDS point scan or TEM.

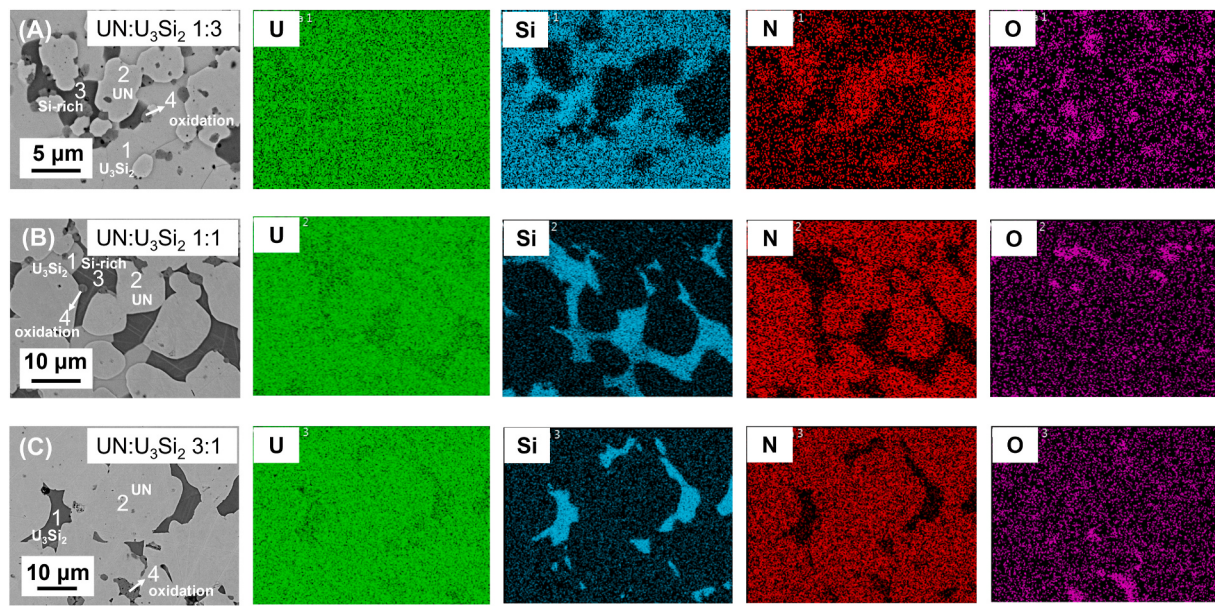


Fig. 3. EDS mappings of the UN + U₃Si₂ composites sintered at 1450 °C: (A) 25 wt% UN + 75 wt% U₃Si₂, (B) 50 wt% UN + 50 wt% U₃Si₂, and (C) 75 wt% UN + 25 wt% U₃Si₂. The elemental mappings confirm that two major phases U₃Si₂ and UN are uniformly distributed. Slight oxidation can be found possibly induced from the SPS sintering or surface oxidation of the densified UN pellets.

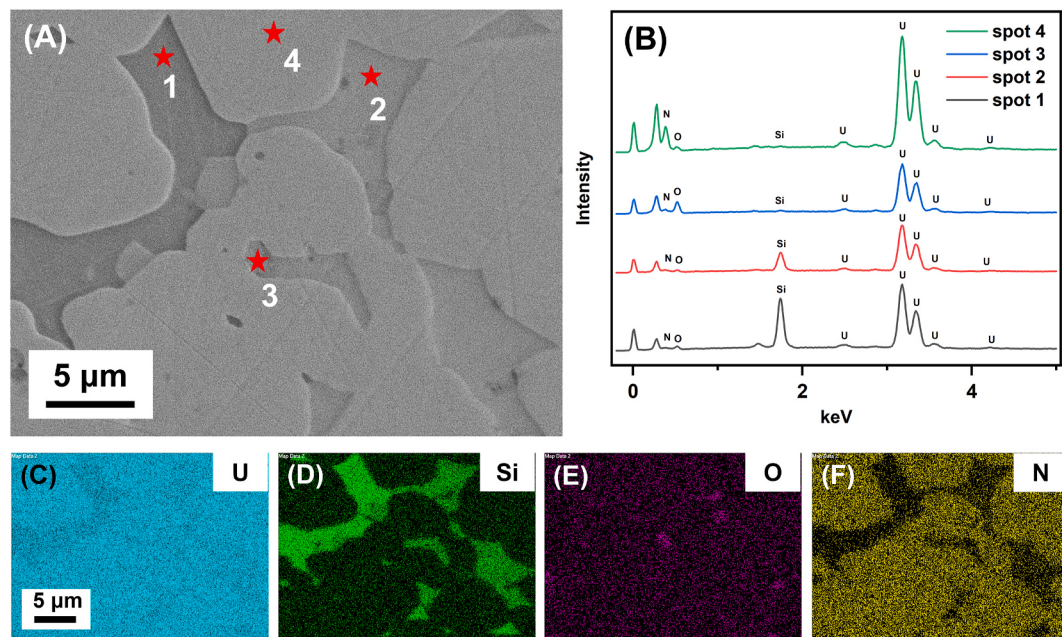


Fig. 4. A SEM image (A) of an enlarged region of the 50 wt% UN – 50 wt% U₃Si₂ and elemental analysis by EDS point scan (B) and mappings (C). Quantitative elemental analysis based on the EDX spectra is summarized in Table 1.

Table 1

The EDS elemental point scan results of the 50% UN + 50% U₃Si₂ specimen showing atomic ratio for each element.

Element	Spot 1	Spot 2	Spot 3	Spot 4
	Atomic%	Atomic%	Atomic%	Atomic%
U	29	34	22	19
Si	43	27	1	0
O	17	17	61	9
N	11	22	17	72

3.2. Mechanical and thermal properties of the composite fuels

Fig. 5 shows SEM images of a representative micro-indentation on each of the UN + U₃Si₂ composite fuels with an increasing weight ratio in UN. Overall, the hardness of each composite fuel is close, ranging from 6.39 GPa to 6.52 GPa. The hardness of these three samples is found to be between the hardness of UN [46] and U₃Si₂ [21], indicating that the hardness of the composites is dependent on the hardness of both compositions. It is also found that the hardness of all composites is closer to the hardness of U₃Si₂, suggesting that the hardness of the UN + U₃Si₂ composite fuels might be dominated by U₃Si₂. The fracture toughness of all the composite fuels ranges from 2.9 to 3.8 MPa m^{1/2}, all of which are

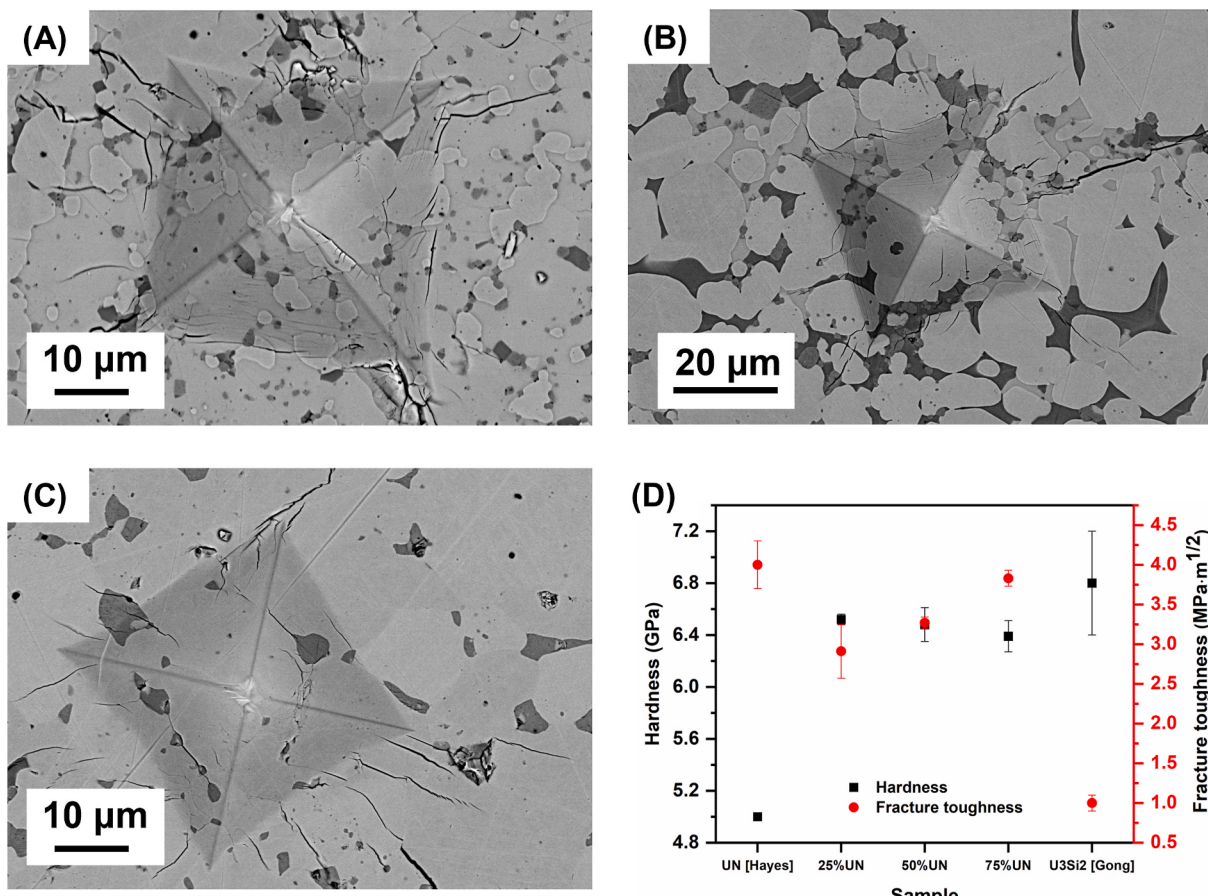


Fig. 5. SEM images of the indentation on the composites: (A) 25 wt% UN + 75 wt% U₃Si₂, (B) 50 wt% UN + 50 wt% U₃Si₂, and (C) 75 wt% UN + 25 wt% U₃Si₂, and (D) hardness and fracture toughness of the three composites, along with data of monolithic UN and U₃Si₂ for comparison.

lower than monolithic UN and higher than monolithic U₃Si₂. The findings suggest that the composite fuels combine the advantages of UN and U₃Si₂ and display a simultaneously high hardness and a much-improved fracture toughness. Fig. 5A shows the indentation of the sample with 25 wt% UN. It seems that many cracks were generated during the micro-indentation testing. At each corner of the indent, there are multiple cracks, some of which propagate towards the diagonal direction of the indentation, while the others propagate along the sides of the indentation. Apart from the cracks, corrugation structure can be seen at the inner wall of the indentation, which can be mitigated with a higher

UN weight ratio.

Thermal diffusivity was evaluated with a LFA with a range of 300–1200 K. Thermal conductivity was calculated subsequently based on the mixing ratio of UN and U₃Si₂. The temperature-dependent values for density and specific heat capacity are mentioned in the experimental details section. The results of these three composite fuels with various weight ratios are shown in Fig. 6. Thermal diffusivity and conductivity data of UN [30] and U₃Si₂ [21] was also included for comparison. First, the thermal diffusivity of U₃Si₂ keeps increasing until 1100 K and then slightly decreases, which is due to the oxidation and possible cracking at

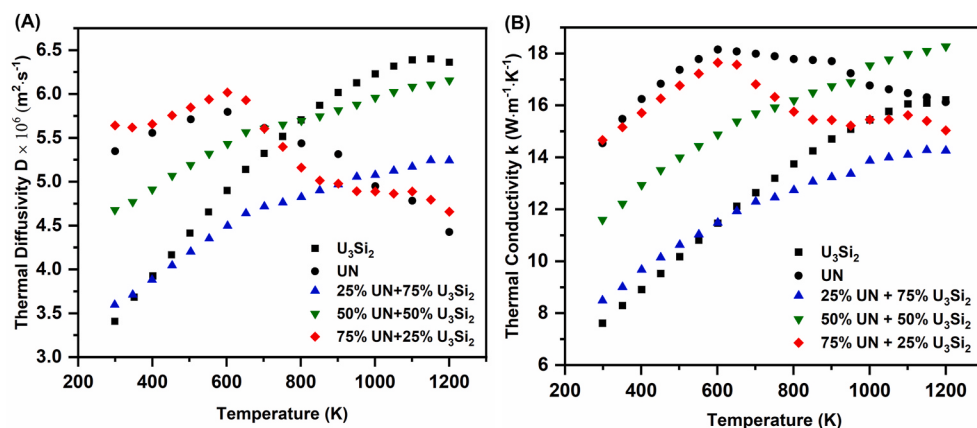


Fig. 6. Thermal diffusivity (A) and thermal conductivity (B) of UN + U₃Si₂ composites with different UN contents, along with these of monolithic UN and U₃Si₂ for comparison.

elevated temperatures. Although the chamber of the LFA was evacuated prior to the testing and high-purity Ar was used as the protection gas during the testing, oxidation still occurred since the chamber is not completely air-tight with degradation of the equipment. On the other hand, the behavior of the thermal conductivity degradation above a critical temperature provides further information on the oxidation behavior as measured by the TGA-DSC measurement. Thermal diffusivity of UN [30] increases with temperature from room temperature until up to 600 K and then starts to drop down with temperature. This was also due to the oxidation as stated before. For three composite fuels, the two samples with 50 wt% U_3Si_2 and 75 wt% U_3Si_2 remain an increasing thermal diffusivity for the whole test, which suggests that U_3Si_2 may play a more important role in determining the thermal diffusivity of the composites. This might be because the phase of U_3Si_2 encapsulates the UN phase and provides additional protection against oxidation. For the specimens with 25% U_3Si_2 , it has an increasing thermal diffusivity up to ~ 600 K, followed by a decreasing trend until the end of the test. This is similar to the behavior of UN, which seems to indicate that UN plays a dominant role in determining the thermal behavior of the sample with 25% U_3Si_2 . Looking at the thermal conductivity of the composite fuels shown in Fig. 6B, it can be observed that all specimens generally follow the same trend as the thermal diffusivity. The thermal conductivity of UN can be found to possess the highest value until ~ 1000 K, where a sudden drop occurred. This might be due to the pulverization of the pellet. For the specimen with 25% U_3Si_2 , its thermal conductivity started to drop at ~ 600 K due to the oxidation of UN. Particularly for the specimen with 50% U_3Si_2 , it shows an increasing trend within the full testing temperature range, suggesting an enhanced oxidation resistance comparing to the specimen with 25% U_3Si_2 . After the temperature reaches 1000 K, this specimen has the highest thermal conductivity among all composite samples, which can be attributed to the synergistic effects of greater oxidation resistance and higher thermal conductivity from the U_3Si_2 and UN phases, respectively. A higher thermal conductivity generally indicates better heat release efficiency, which is a merit for nuclear fuels to ensure a safe operational condition, especially at elevated temperatures.

3.3. Oxidation resistance of the composite fuels

Fig. 7 shows the oxidation behavior of three composite fuels sintered with SPS, all of which demonstrate excellent oxidation resistance that can be judged from the higher onset temperature and prolonged time to

full oxidation. The onset temperature of all samples is around 540 °C, which is slightly higher than those of monolithic nanocrystalline (referred as nc-hereafter) U_3Si_2 [21] (510 °C) and microcrystalline (referred as mc-hereafter) U_3Si_2 (520 °C), and much higher than that (450 °C) of monolithic UN sintered with SPS [30] at 1600 °C. This result suggests that the composite fuels without microcracking in this study possess much better oxidation resistance than monolithic UN, and the oxidation resistance is mainly dominated by U_3Si_2 in the UN- U_3Si_2 composite. The slightly higher onset temperature for the UN- U_3Si_2 composites than monolithic U_3Si_2 (mc- or nc- U_3Si_2) reported in our previous study [21] could be attributed to the micro-strain accumulation on the U_3Si_2 phase. Particularly, due to a large mismatch in the thermal expansion between UN and U_3Si_2 , a non-uniform strain field is expected during SPS sintering. The much larger thermal expansion coefficient makes the silicide phase contracting significantly during the cooling processing, resulting in a tensile stress applied on the silicide grains. The tensile stress was reported in our previous study on SPS-densified mc- U_3Si_2 with observable lattice expansion, which profoundly impacts the oxidation resistance of the fuel matrix. By thermal annealing, the tensile stress of the mc- U_3Si_2 can be relaxed, increasing the onset temperature from 520 to 560 °C [21]. Therefore, the stress relaxation during the controlled cooling processing of the SPS sintering not only mitigates the micro-cracking in the UN- U_3Si_2 composite fuel matrix but also increases their oxidation resistance.

Johnson et al. [47] reported the onset temperature of the composite fuel UN+10% U_3Si_2 , which is 450 °C and is lower than the composites reported here. The authors [47] reported that the oxidation behavior of the composite is very close to that of the UN sample with 99.8% TD. The dominant effect of UN phase on oxidation behavior could be attributed to possible microcracking and limited U_3Si_2 content in the composite. Costa et al. [22] reported the oxidation of UN/ U_2N_3 - UO_2 composites, where the authors explored the potentials of utilizing oxide phases as a protection for nitride phases. The onset temperature of UN- UO_2 samples is in the range of 283–320 °C, which varies according to the content of UO_2 . Increasing the amount of UN leads to a reduction in the onset temperature, possibly due to the reduction in the density of the sintered pellets and the lower oxidation onset temperature of UN than UO_2 . The onset temperature of U_3Si_2 + UO_2 composites was reported to be in the range of 260 °C to 480 °C, increasing with the content of U_3Si_2 . These comparisons suggest that the composites of UN- U_3Si_2 sintered in this study without microcracking display improved oxidation resistance with the onset oxidation temperature better than these of UN, U_3Si_2 , and their composite fuels reported in literature.

4. Conclusions

In summary, UN and U_3Si_2 composite fuels with various compositions were fabricated with controlled sintering and cooling processes, which helped to greatly mitigate the micro-cracking induced by thermal mismatch found in other work. Systematic characterization including SEM, XRD, and EDS was carried out to understand the microstructures of the sintered composites. The thermomechanical properties of all specimens were measured by microhardness testing, laser flash apparatus, and thermogravimetric analysis to evaluate the potential of UN + U_3Si_2 as candidates of ATFs. The composite with 50 wt% UN and 50 wt% U_3Si_2 exhibits enhanced strength and fracture toughness simultaneously, as well as an improved thermal conductivity that increases with temperature. Besides, all composites are found to possess an onset temperature close to 540 °C, which is higher than monolithic UN, U_3Si_2 , as well as UO_2 , indicating a well-improved oxidation resistance. Further experiments, including water steam testing and autoclave testing, are being carried out to understand their corrosion resistance and also to evaluate the performance of these composites under extreme conditions.

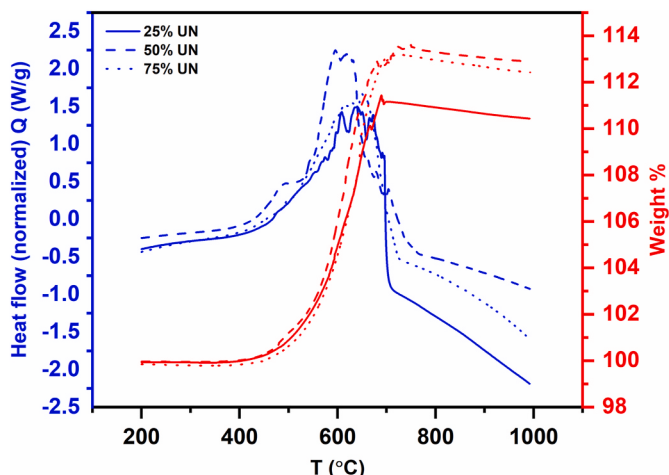


Fig. 7. TGA/DSC data of the three UN + U_3Si_2 composites. All samples have an oxidation onset temperature around 540 °C, which is significantly higher than that of monolithic UN, suggesting improved oxidation resistance and the merit of synergizing two leading fuels into composite forms for enhanced fuel properties.

Declaration of competing interest

The authors declare that they have no known competing financial interests or personal relationships that could have appeared to influence the work reported in this paper.

Data availability

The data that support the findings of this study are available from the corresponding author upon reasonable request.

Acknowledgement

This work was supported by the US Department of Energy's (DOE's) Office of Nuclear Energy under Nuclear Energy University Programs (award numbers: DE-NE0008947 and DE-NE0008532) and by Westinghouse Electric Company under the DOE ATF program supported by the Department of Energy under an Award Number of DE-NE0008824. This report was prepared as an account of work sponsored by an agency of the United States Government. Neither the United States Government nor any agency thereof, nor any of their employees, makes any warranty, express or implied, or assumes any legal liability or responsibility for the accuracy, completeness, or usefulness of any information, apparatus, product, or process disclosed, or represents that its use would not infringe privately owned rights. Reference herein to any specific commercial product, process, or service by trade name, trademark, manufacturer, or otherwise does not necessarily constitute or imply its endorsement, recommendation, or favoring by the United States Government or any agency thereof. The views and opinions of authors expressed herein do not necessarily state or reflect those of the United States Government or any agency thereof.

References

- [1] J. Carmack, F. Goldner, S.M. Bragg-Sitton, L.L. Snead, Overview of the US DOE Accident Tolerant Fuel Development Program, Idaho National Laboratory (INL), 2013.
- [2] J. Harding, D. Martin, A recommendation for the thermal conductivity of UO₂, *J. Nucl. Mater.* 166 (1989) 223–226.
- [3] D. Martin, A re-appraisal of the thermal conductivity of UO₂ and mixed (U, Pu) oxide fuels, *J. Nucl. Mater.* 110 (1982) 73–94.
- [4] G. Hyland, Thermal conductivity of solid UO₂: critique and recommendation, *J. Nucl. Mater.* 113 (1983) 125–132.
- [5] K. Kurosaki, Y. Saito, H. Muta, M. Uno, S. Yamanaka, Nanoindentation studies of UO₂ and (U, Ce) O₂, *J. Alloys Compd.* 381 (2004) 240–244.
- [6] E. Kardoulaki, D.M. Frazer, J.T. White, U. Carvajal, A.T. Nelson, D.D. Byler, T. A. Saleh, B. Gong, T. Yao, J. Lian, K.J. McClellana, Fabrication and thermophysical properties of UO₂-UB2 and UO₂-UB4 composites sintered via spark plasma sintering, *J. Nucl. Mater.* 544 (2021) 152690.
- [7] B. Gong, D. Frazer, T. Yao, P. Hosemann, M. Tonks, J. Lian, Nano-and micro-indentation testing of sintered UO₂ fuel pellets with controlled microstructure and stoichiometry, *J. Nucl. Mater.* 516 (2019) 169–177.
- [8] T. Yao, S.M. Scott, G. Xin, J. Lian, TiO₂ doped UO₂ fuels sintered by spark plasma sintering, *J. Nucl. Mater.* 469 (2016) 251–261.
- [9] W. Miekeley, F. Felix, Effect of stoichiometry on diffusion of xenon in UO₂, *J. Nucl. Mater.* 42 (1972) 297–306.
- [10] T. Yao, S.M. Scott, G. Xin, B. Gong, J. Lian, Dense nanocrystalline UO_{2+x} fuel pellets synthesized by high pressure spark plasma sintering, *J. Am. Ceram. Soc.* 101 (2018) 1105–1115.
- [11] J. Arborelius, K. Backman, L. Hallstadius, M. Limbaeck, J. Nilsson, B. Rebensdorff, G. Zhou, K. Kitano, R. Loefstroem, G. Roennberg, Advanced doped UO₂ pellets in LWR applications, *J. Nucl. Sci. Technol.* 43 (2006) 967–976.
- [12] M.W.D. Cooper, C.R. Stanek, D. Andersson, The role of dopant charge state on defect chemistry and grain growth of doped UO₂, *Acta Mater.* 150 (2018) 403–413.
- [13] A. Sengupta, C. Basak, T. Jarvis, R. Bhagat, V. Pandey, S. Majumdar, Effect of titania addition on hot hardness of UO₂, *J. Nucl. Mater.* 325 (2004) 141–147.
- [14] S. Ishimoto, M. Hirai, K. Ito, Y. Korei, Thermal conductivity of UO₂-BeO pellet, *J. Nucl. Sci. Technol.* 33 (1996) 134–140.
- [15] D.A. Lopes, S. Uygur, K. Johnson, Degradation of UN and UN-U3Si₂ pellets in steam environment, *J. Nucl. Sci. Technol.* 54 (2017) 405–413.
- [16] B. Gong, T. Yao, P. Lei, L. Cai, K.E. Metzger, E.J. Lahoda, F.A. Boylan, A. Mohamad, J. Harp, A.T. Nelson, U3Si₂ and UO₂ composites densified by spark plasma sintering for accident-tolerant fuels, *J. Nucl. Mater.* 534 (2020) 152147.
- [17] J.T. White, A.T. Nelson, J.T. Dunwoody, D.J. Safarik, K.J. McClellan, Corrigendum to "thermophysical properties of U3Si₂ to 1773 K", *J. Nucl. Mater.* (2016) 484.
- [18] D.J. Antonio, K. Shrestha, J.M. Harp, C.A. Adkins, Y. Zhang, J. Carmack, K. Gofryk, Thermal and transport properties of U3Si₂, *J. Nucl. Mater.* 508 (2018) 154–158.
- [19] D.A. Lopes, S. Uygur, K. Johnson, Degradation of UN and UN-U3Si₂ pellets in steam environment, *J. Nucl. Sci. Technol.* 54 (2017) 405–413.
- [20] E.S. Wood, J.T. White, C.J. Grote, A.T. Nelson, U3Si₂ behavior in H₂O: Part I, flowing steam and the effect of hydrogen, *J. Nucl. Mater.* 501 (2018) 404–412.
- [21] B. Gong, T. Yao, P. Lei, J. Harp, A.T. Nelson, J. Lian, Spark plasma sintering (SPS) densified U3Si₂ pellets: microstructure control and enhanced mechanical and oxidation properties, *J. Alloys Compd.* 825 (2020) 154022.
- [22] D.R. Costa, M. Hedberg, S.C. Middleburgh, J. Wallenius, P. Olsson, D.A. Lopes, Oxidation of UN/U2N3-UO₂ composites: an evaluation of UO₂ as an oxidation barrier for the nitride phases, *J. Nucl. Mater.* 544 (2021) 152700.
- [23] M. Grolke, M. Steinbrück, J. Stuckert, Steam and air oxidation behavior of nuclear fuel claddings at severe accident conditions, *MRS Online Proc. Libr.* 1264 (2010) 1–6.
- [24] B. Gong, L. Cai, P. Lei, K.E. Metzger, E.J. Lahoda, F.A. Boylan, K. Yang, J. Fay, J. Harp, J. Lian, Cr-doped U3Si₂ composite fuels under steam corrosion, *Corrosion Sci.* 177 (2020) 109001.
- [25] Y. Takahashi, M. Murabayashi, Y. Akimoto, T. Mukaibo, Uranium mononitride: heat capacity and thermal conductivity from 298 to 1000 K, *J. Nucl. Mater.* 38 (1971) 303–308.
- [26] S. Hayes, J. Thomas, K. Peddicord, Material property correlations for uranium mononitride: III. Transport properties, *J. Nucl. Mater.* 171 (1990) 289–299.
- [27] T. Kikuchi, T. Takahashi, S. Nasu, Porosity dependence of thermal conductivity of uranium mononitride, *J. Nucl. Mater.* 45 (1973) 284–292.
- [28] C. Alexander, J. Ogden, W. Pardue, Volatilization characteristics of uranium mononitride, *J. Nucl. Mater.* 31 (1969) 13–24.
- [29] L. He, M. Khafizov, C. Jiang, B. Tyburska-Püschel, B.J. Jaques, P. Xiu, P. Xu, M. K. Meyer, K. Sridharan, D.P. Butt, Phase and defect evolution in uranium-nitrogen-oxygen system under irradiation, *Acta Mater.* 208 (2021) 116778.
- [30] K. Yang, E. Kardoulaki, D. Zhao, B. Gong, A. Broussard, K. Metzger, J.T. White, M. R. Sivack, K.J. McClellan, E.J. Lahoda, J. Lian, Uranium nitride (UN) pellets with controllable microstructure and phases – fabrication by spark plasma sintering and their thermal-mechanical and oxidation properties, *J. Nucl. Mater.* (2021) submitted for publication.
- [31] J.K. Watkins, D.P. Butt, B.J. Jaques, Microstructural degradation of UN and UN-UO₂ composites in hydrothermal oxidation conditions, *J. Nucl. Mater.* 518 (2019) 30–40.
- [32] K.D. Johnson, A.M. Raftery, D.A. Lopes, J. Wallenius, Fabrication and microstructural analysis of UN-U3Si₂ composites for accident tolerant fuel applications, *J. Nucl. Mater.* 477 (2016) 18–23.
- [33] J.T. White, A.W. Travis, J.T. Dunwoody, A.T. Nelson, Fabrication and thermophysical property characterization of UN/U3Si₂ composite fuel forms, *J. Nucl. Mater.* 495 (2017) 463–474.
- [34] L.H. Ortega, B.J. Blamer, J.A. Evans, S.M. McDeavitt, Development of an accident-tolerant fuel composite from uranium mononitride (UN) and uranium sesquisilicide (U3Si₂) with increased uranium loading, *J. Nucl. Mater.* 471 (2016) 116–121.
- [35] D. Lopes, T. Wilson, V. Kocevski, E. Moore, T. Besmann, E.S. Wood, J. White, A. Nelson, S. Middleburgh, A. Claisse, Experimental and computational assessment of USIN ternary phases, *J. Nucl. Mater.* 516 (2019) 194–201.
- [36] J.M. Harp, P.A. Lessing, R.E. Hoggan, Uranium silicide pellet fabrication by powder metallurgy for accident tolerant fuel evaluation and irradiation, *J. Nucl. Mater.* 466 (2015) 728–738.
- [37] E.S. Wood, J.T. White, A.T. Nelson, Oxidation behavior of U-Si compounds in air from 25 to 1000 C, *J. Nucl. Mater.* 484 (2017) 245–257.
- [38] P. Chantikul, G. Anstis, B.R. Lawn, D. Marshall, A critical evaluation of indentation techniques for measuring fracture toughness: II, strength method, *J. Am. Ceram. Soc.* 64 (1981) 539–543.
- [39] T. Wang, N. Qiu, X. Wen, Y. Tian, J. He, K. Luo, X. Zha, Y. Zhou, Q. Huang, J. Lang, First-principles investigations on the electronic structures of U3Si₂, *J. Nucl. Mater.* 469 (2016) 194–199.
- [40] S. Hayes, J. Thomas, K. Peddicord, Material property correlations for uranium mononitride: ii. mechanical properties, *J. Nucl. Mater.* 171 (1990) 271–288.
- [41] S. Hayes, J. Thomas, K. Peddicord, Material property correlations for uranium mononitride: I. Physical properties, *J. Nucl. Mater.* 171 (1990) 262–270.
- [42] H. Shimizu, THE PROPERTIES and IRRADIATION BEHAVIOR OF U \$ Sub 3\$ Si \$ Sub 2\$, Atomics International, Canoga Park, Calif., 1965.
- [43] R. Liu, W. Zhou, J. Cai, Multiphysics modeling of accident tolerant fuel-cladding U3Si₂-FeCrAl performance in a light water reactor, *Nucl. Eng. Des.* 330 (2018) 106–116.
- [44] K.D. Johnson, D.A. Lopes, Grain growth in uranium nitride prepared by spark plasma sintering, *J. Nucl. Mater.* 503 (2018) 75–80.
- [45] E. Kardoulaki, D. Byler, J. Bárta, K. McClellan, Tri-arc growth and characterization of U3Si₂ and U3Si₅ single crystals, *J. Cryst. Growth* 558 (2021) 126025.
- [46] S.L. Hayes, J.K. Thomas, K.L. Peddicord, Material property correlations for uranium mononitride: ii. mechanical properties, *J. Nucl. Mater.* 171 (1990) 271–288.
- [47] K. Johnson, V. Ström, J. Wallenius, D.A. Lopes, Oxidation of accident tolerant fuel candidates, *J. Nucl. Sci. Technol.* 54 (2017) 280–286.